Optical Engineering

OpticalEngineering.SPIEDigitalLibrary.org

Imitation of optical coherence tomography images by wave Monte Carlo-based approach implemented with the Leontovich–Fock equation

Andrey D. Bulygin
Denis A. Vrazhnov
Elena S. Sim
Igor Meglinski
Yury V. Kistenev

SPIE.

Andrey D. Bulygin, Denis A. Vrazhnov, Elena S. Sim, Igor Meglinski, Yury V. Kistenev, "Imitation of optical coherence tomography images by wave Monte Carlo-based approach implemented with the Leontovich–Fock equation," *Opt. Eng.* **59**(6), 061626 (2020), doi: 10.1117/1.OE.59.6.061626

Downloaded From: https://www.spiedigitallibrary.org/journals/Optical-Engineering on 09 Apr 2020
Terms of Use: https://www.spiedigitallibrary.org/terms-of-use

Imitation of optical coherence tomography images by wave Monte Carlo-based approach implemented with the Leontovich–Fock equation

Andrey D. Bulygin,[a,b] Denis A. Vrazhnov,[a,c] Elena S. Sim,[a] Igor Meglinski,[a,d,e,f] and Yury V. Kistenev[a,*]

[a]National Research Tomsk State University, Interdisciplinary Laboratory of Biophotonics, Tomsk, Russia

[b]V.E. Zuev Institute of Atmospheric Optics SB RAS, Laboratory of Nonlinear Optical Interactions, Tomsk, Russia

[c]Institute of Strength Physics and Materials Science SB RAS, Laboratory of Molecular Imaging and Photoacoustics, Tomsk, Russia

[d]University of Oulu, Optoelectronics and Measurement Techniques Laboratory, Oulu, Finland

[e]Aston University, School of Engineering and Applied Science, Birmingham, United Kingdom

[f]Aston University, School of Life and Health Sciences, Birmingham, United Kingdom

Abstract. We present a computational modeling approach for imitation of the time-domain optical coherence tomography (OCT) images of biotissues. The developed modeling technique is based on the implementation of the Leontovich–Fock equation into the wave Monte Carlo (MC) method. We discuss the benefits of the developed computational model in comparison to the conventional MC method based on the modeling of OCT images of a nevus. The developed model takes into account diffraction on bulk-absorbing microstructures and allows consideration of the influence of the amplitude–phase profile of the wave beam on the quality of the OCT images. The selection of optical parameters of modeling medium, used for simulation of optical radiation propagation in biotissues, is based on the results obtained experimentally by OCT. The developed computational model can be used for imitation of the light waves propagation both in time-domain and spectral-domain OCT approaches. © *2020 Society of Photo-Optical Instrumentation Engineers (SPIE)* [DOI: 10.1117/1.OE.59.6.061626]

Keywords: optical coherence tomography; Monte Carlo method; Leontovich–Fock equation; biological tissue; imaging.

Paper 191644SS received Nov. 27, 2019; accepted for publication Feb. 12, 2020; published online Feb. 28, 2020.

1 Introduction

The time-domain optical coherence tomography (OCT) is based on the interference of low-coherent optical radiation backscattered from medium inhomogeneities with the reference beam and is used extensively for structural and functional imaging of biological tissues.[1] The interpretation of the OCT images and quantitative assessment of the structural and optical parameters of turbid scattering biological tissues requires the development of realistic computational models for ultimate understanding of the formation of OCT images.

Typically, for modeling of the light propagation in biological tissues and tissue-like scattering media, including mimicking of OCT images, either a plane wave approximation[2–5] or the conventional Monte Carlo (MC) method[6–15] is used. In fact, both of these approaches have some disadvantages. The vector MC method takes into account the wave phenomena, such as diffraction and/or coherence, utilizing artificial methods developed outside of the original model of radiation transfer, as the individual photon trajectories are counted independently.

Modeling of light propagation within the random medium based on the Huygens–Fresnel principle allows considering diffraction but only for bulk inhomogeneities with sharp

*Address all correspondence to Yury V. Kistenev, E-mail: yuk@iao.ru

0091-3286/2020/$28.00 © 2020 SPIE

Downloaded From: https://www.spiedigitallibrary.org/journals/Optical-Engineering on 09 Apr 2020
Terms of Use: https://www.spiedigitallibrary.org/terms-of-use

boundaries.[16–21] The propagation of light within biological tissue is modeled typically by a set of particles also known as "photon packets" (Ref. 22). The Huygens–Fresnel principle approach has a high computational complexity since the wavefront is considered as a set of point sources, described by differential equation.[23]

Using the Maxwell equations for the OCT simulations is suitable for modeling complex (profiled) laser beams.[24–29] However, it is very time-consuming, even using parallel algorithms,[30–32] and requires allocation of massive computer resources that significantly limits the spatial area of interest.

An approach based on a quasioptics approximation has been developed, where stochastic medium inhomogeneity was modeled by a set of phase screens with a random spatial distribution of the phase incursion.[33] A model of optical wave radiation propagation in a biotissue based on the Leontovich–Fock stochastic equation also referred to as a quasi-optics approximation was proposed.[34] The advantage of the model is that it provides an effective numerical implementation. Applying this approach for the simulation of OCT images of biological tissues requires a generalization of the model for the case of a partially coherent beam. The latter can be implemented as a set of statistical tests, where each optical wave with a given random phase distribution at the entrance to the medium propagates independently, and finally, their superposition is counted. By analogy with the conventional MC, this approach is known as the wave MC.[35]

To imitate OCT signal formation by MC, it is necessary to calculate the propagation of the backward wave reflected from the boundaries of structural inhomogeneities localized within the medium. The combination of the wave MC method and the wave equation in the quasioptics approximation potentially makes it possible to simulate with reasonable computing resource requirements of the wave beams with a complex amplitude–phase profile and to take into account diffraction. In the current paper, utilizing the Leontovich–Fock stochastic parabolic equation, we introduce a new wave MC-based model for simulation of the time-domain OCT signals and 2D images.

2 Approach to Modeling of Biological Tissue Visualization Structure by the OCT Method

2.1 *Model of Optical Radiation Propagation in Biological Tissue*

Let us denote the electric field of an optical wave in the following form:

$$E(\mathbf{r},t)=\psi(\mathbf{r},t)e^{i\omega_0 t}, \tag{1}$$

where $\omega_0 = k_0 c$ is the carrier (central) frequency. Then, the corresponding Helmholtz equation for a randomly inhomogeneous medium is calculated as

$$\Delta\psi(\mathbf{r},t)+k_0^2\psi(\mathbf{r},t)=-k_0^2(\langle\varepsilon\rangle+\delta\varepsilon)\psi(\mathbf{r},t), \tag{2}$$

where $\delta\varepsilon$ is the dielectric permeability fluctuations ε and $\Delta\equiv\nabla^2$ is the Laplace operator. Further, time dependence further will be omitted.

Taken into account that $\psi(\mathbf{r})$ is presented as $\psi(\mathbf{r})=U(\mathbf{r})e^{ik_0 z}$, Eq. (2) in a quasioptics approximation takes the form:

$$2ik_0\frac{\partial}{\partial z}U(\mathbf{r}_\perp,z)+\Delta_\perp U(\mathbf{r}_\perp,z)=-k_0^2(\langle\varepsilon\rangle+\delta\varepsilon)U(\mathbf{r}_\perp,z). \tag{3}$$

Assuming that $\nabla\langle\varepsilon\rangle=0$, Eq. (3) can be simplified as

$$\frac{\partial}{\partial z}\tilde{U}(\mathbf{r}_\perp,z,t)=\frac{i}{4}\Delta_\perp\tilde{U}+i\tilde{n}(\mathbf{r}_\perp,z)\tilde{U}, \tag{4}$$

where $\tilde{n}(\mathbf{r}_\perp,z)\equiv k_0 L_R\tilde{n}_c$ is the normalized complex refractive index of a medium; $\tilde{n}_c=n+\delta\tilde{n}$ is the complex refractive index of the medium, where the real part represents the phase incursion, and the imaginary one characterizes absorption, $\delta\tilde{n}$ is the medium refractive index fluctuations; $L_R=k_0R_0^2/2$ is the Rayleigh length equal to half the distance at which a collimated beam

Downloaded From: https://www.spiedigitallibrary.org/journals/Optical-Engineering on 09 Apr 2020
Terms of Use: https://www.spiedigitallibrary.org/terms-of-use

with a Gaussian shape of the intensity distribution in the cross-section doubles in diameter; R_0 is the initial radius of the beam; $k_0 = 2\pi/\lambda_0$ is the wavenumber at the central wavelength λ_0; $r_\perp \to r_\perp/R_0$ is dimensionless transverse coordinate; $z \to z/L_R$ is the dimensionless coordinate along the beam propagation direction; $\nabla_\perp$ is the Nabla operator, which includes differentiation only over transverse coordinates; $\tilde{U}(\mathbf{r}_\perp, z, t) = \tilde{A}(\mathbf{r}_\perp, z, t)e^{i\tilde{\varphi}(\mathbf{r}_\perp, z, t)}$ is the slowly changing complex amplitude of the light field normalized to its maximum initial value; $\tilde{A}(\mathbf{r}_\perp, z, t)$ and $\tilde{\varphi}(\mathbf{r}_\perp, z, t)$ are, respectively, amplitude and phase. Hereinafter, the wave symbol denotes a random function.

Let us describe the phase $\tilde{\varphi}(t)$ by a random function with the Lorentzian shape of the spectrum fluctuations:[36]

$$\langle \tilde{\varphi}(t-\tau)\tilde{\varphi}(t)\rangle = D_\varphi e^{-\tau/T_{\text{corr}}}, \tag{5}$$

where T_{corr} defines the temporal coherence of the optical wave radiation and determines the longitudinal resolution in OCT; and D_φ is the phase fluctuation dispersion.

The field amplitude is defined as follows:

$$\tilde{A}(\mathbf{r}_\perp, t) = A(\mathbf{r}_\perp, t) + \delta\tilde{A}(\mathbf{r}_\perp, t).$$

Similar to Eq. (5), the amplitude fluctuations $\delta\tilde{A}(t)$ are described as follows:

$$\langle \delta\tilde{A}(t-\tau)\delta\tilde{A}(t)\rangle = D_A e^{-\tau/T_{\text{corr}}},$$

where D_A is the amplitude fluctuation dispersion (usually, $D_A \ll 1$), $\langle \delta A(t)\rangle = 0$.

The phase $\tilde{\varphi}$ can be found from the Leontovich–Fock equation:

$$\partial_z\tilde{\varphi} = -\partial_z \operatorname{Im}(\ln(\tilde{U})) = \tilde{n}(\mathbf{r}_\perp, z) + \frac{\nabla_\perp^2|\tilde{A}|}{4|\tilde{A}|}. \tag{6}$$

The simulation of time-domain OCT images of biotissue was carried out based on Eqs. (4)–(6) for a set of realizations of random optical waves with given characteristics at the entrance to the medium. Then, the interference of reference wave and the superposition of the waves backreflected/scattered from structural inhomogeneities of the biological tissue during an observation time T are counted as follows:

$$I_{\text{oct}}(\mathbf{r}_\perp, L) = \int_T \mathrm{d}t\langle \tilde{A}_{sc}(\mathbf{r}_\perp, t)\tilde{A}_0(\mathbf{r}_\perp, t - n_0L/c)\operatorname{Re}(e^{i(\tilde{\varphi}_{sc}(t)-\tilde{\varphi}(t-n_0L/c))})\rangle/T, \tag{7}$$

where $\tilde{A}_{\text{sc}}$ and $\tilde{\varphi}_{\text{sc}}(t)$ are the amplitude and phase of the optical wave backscattered from the tissue; $\tilde{A}_0$ is the amplitude of the source light field; L is the difference of the interferometer arms lengths (a variable parameter that determines the position of the observed layer in the medium in the time-domain OCT); c is the speed of light; and n_0 is the refractive index of air.

2.2 *Model of Randomly Inhomogeneous Medium*

We use the following designations:

$$\langle \delta\tilde{n}(\mathbf{r})\delta\tilde{n}(\mathbf{r}-\delta\mathbf{r})\rangle = C(\delta\mathbf{r}) = \int_{V_k} e^{-i\mathbf{k}\delta\mathbf{r}}C(\mathbf{k})\mathrm{d}\mathbf{k}.$$

where $\mathbf{r} = \mathbf{r}_\perp + z\cdot\vec{e}_z$, where $\vec{e}_z$ is the Cartesian coordinate system unit vector and $C(\mathbf{k})$ is defined in the frame of the phenomenological model:[37]

$$C(\mathbf{k}) = C_0\frac{1}{(1 + l_c^2|\mathbf{k}|^2)^{D_f/2}}. \tag{8}$$

The medium model parameters include the correlation radius l_c, the magnitude D_f of refractive index fluctuations, and the dispersion of refractive index fluctuations C_0. Setting these parameters determines the type of biological tissue.[38–43]

Downloaded From: https://www.spiedigitallibrary.org/journals/Optical-Engineering on 09 Apr 2020
Terms of Use: https://www.spiedigitallibrary.org/terms-of-use

Here and following, we use the following notation for triple integrals:

$$\int_{V_k} f(\mathbf{k})\mathrm{d}\mathbf{k} \equiv \int_{-\infty}^{\infty}\int_{-\infty}^{\infty}\int_{-\infty}^{\infty} f(k_x, k_y, k_z)\mathrm{d}k_x\,\mathrm{d}k_y\,\mathrm{d}k_z.$$

The "volume" V is defined in a corresponding 3D real number space.

Let us establish a link between the statistical characteristics of the medium parameters and the parameters of the scattering indicatrix in the radiation transfer equation (RTE), which is a typical base of the conventional MC approach.

Let us designate the two-point statistical moment (average of the product of the optical wave amplitudes in two spatial points $\mathbf{r}_1$ and $\mathbf{r}_2$), i.e., to the second-order coherence function as follows:

$$\Gamma_2(\mathbf{R}, \delta\mathbf{r}) = \langle U(\mathbf{R}+\delta\mathbf{r})U^*(\mathbf{R}-\delta\mathbf{r})\rangle_{\delta\varepsilon}.$$

Here, $\mathbf{R} = (\mathbf{r}_1 + \mathbf{r}_2)/2$; $\delta\mathbf{r} = (\mathbf{r}_1 - \mathbf{r}_2)/2)$. Differentiating Γ_2 on $\nabla_{\mathbf{R}}\nabla_{\delta\mathbf{r}}$, we get

$$\nabla_{\mathbf{R}}\nabla_{\delta\mathbf{r}}\Gamma_2 = \frac{1}{2}k_0^2\langle\delta\varepsilon(\mathbf{R}+\delta\mathbf{r})U(\mathbf{R}+\delta\mathbf{r})U^*(\mathbf{R}-\delta\mathbf{r}) - \delta\varepsilon(\mathbf{R}-\delta\mathbf{r})U(\mathbf{R}+\delta\mathbf{r})U^*(\mathbf{R}-\delta\mathbf{r})\rangle_{\delta\varepsilon}. \quad (9)$$

Taking into account that $\delta\varepsilon$ is the random isotropic homogeneous Gaussian distribution, and integrating Eq. (9) in parts, we obtain

$$i\nabla_{\mathbf{R}}\nabla_{\delta\mathbf{r}}\Gamma_2 = k_0^2(\langle\delta\varepsilon(\mathbf{R}-\delta\mathbf{r})\delta\varepsilon(\mathbf{R}+\delta\mathbf{r})\rangle)\Gamma_2.$$

Presenting the function Γ_2 by Wigner function:

$$J(\mathbf{R}, \mathbf{k}) = \int_{V_r} \Gamma_2(\mathbf{R}, \delta\mathbf{r})e^{-i\mathbf{k}\delta\mathbf{r}}\mathrm{d}\delta\mathbf{r},$$

which gives us the following:

$$\mathbf{k}\nabla_{\mathbf{R}}J(\mathbf{R}, \mathbf{k}) = \int_{V_k} \Theta(\mathbf{k}-\mathbf{k}')J(\mathbf{R}, \mathbf{k}')\mathrm{d}\mathbf{k}', \quad (10)$$

where $\Theta(\mathbf{k}-\mathbf{k}') = k_0^2\int_{V_r} e^{-i(\mathbf{k}-\mathbf{k}')\delta\mathbf{r}}\langle\delta\varepsilon(R-\delta\mathbf{r})\delta\varepsilon(R+\delta\mathbf{r})\rangle\mathrm{d}\delta\mathbf{r} = \frac{k_0^2}{4}C(\mathbf{k}-\mathbf{k}')$.

Further, assuming that the Wigner function J localized inside a sphere $|\mathbf{k}| = k_0$. Thus,

$$J(\mathbf{R}, \mathbf{k}) \approx \delta(|\mathbf{k}| - k_0)I_J(\mathbf{R}, \mathbf{k}), \quad (11)$$

where $I_J(\mathbf{R}, \mathbf{k})$ is the brightness function. By denoting $\mathbf{s} \equiv \mathbf{k}/k_0$, omit further the dependence of $I_J(\mathbf{R}, \mathbf{s}k_0)$ on k_0, and multiplying Eq. (10) on $|\mathbf{k}|^2 d|\mathbf{k}|$ and integrating, we obtain

$$\mathbf{s}\nabla_{\mathbf{R}}I_J(\mathbf{R}, \mathbf{s}) = \frac{k_0^2}{4}\int_{S'^2}\left(\int_0^{\infty} C(\mathbf{s}|\mathbf{k}| - \mathbf{s}'k_0)|\mathbf{k}|^2 d|\mathbf{k}|\right)I_J(\mathbf{R}, \mathbf{s}')\mathrm{d}\mathbf{s}'. \quad (12)$$

Comparing Eq. (12) with the RTE,[40]

$$\mathbf{s}\nabla_{\mathbf{R}}I_J(\mathbf{R}, \mathbf{s}) = \frac{\mu_{\mathrm{sc}}}{4\pi}\int_{S'^2} p(\mathbf{s}, \mathbf{s}')I_J(\mathbf{R}, \mathbf{s}')\mathrm{d}\mathbf{s}', \quad (13)$$

we can conclude that

$$\frac{\mu_{\mathrm{sc}}}{4\pi}p(\mathbf{s}, \mathbf{s}') = \frac{k_0^2}{4}\int_0^{\infty} C(\mathbf{s}|\mathbf{k}| - \mathbf{s}'k_0)|\mathbf{k}|^2\mathrm{d}|\mathbf{k}|, \quad (14)$$

where μ_{sc} is the scattering cross-section, $\mathrm{p}(\mathbf{s}, \mathbf{s}')$ is the scattering phase function described by Heney–Greenstein formula:[44]

Downloaded From: https://www.spiedigitallibrary.org/journals/Optical-Engineering on 09 Apr 2020
Terms of Use: https://www.spiedigitallibrary.org/terms-of-use

$$p(\mathbf{s}, \mathbf{s}') = \frac{1 - g^2}{[1 + g^2 - g\cos(\theta)]^{3/2}}, \tag{15}$$

where $\mathbf{s} \cdot \mathbf{s}' = \cos(\theta)$ is the scalar product of unit the vectors, and g is the anisotropy scattering parameter. This function is often used in MC simulation of optical radiation propagation in tissue. From a theoretical point of view, the constraints of the Heney–Greenstein formula are associated with a discrepancy for anisotropic media, but, in practice, this approach reproduces the experimental data well enough.[45]

Substituting Eq. (14) with Eq. (8):

$$\mathrm{p}(\boldsymbol{s}, \boldsymbol{s}') = \frac{k_0^2 \pi}{\mu_{\mathrm{sc}}} \int_0^{\infty} \frac{C_0}{(1 + (l_c k_0)^2 (|\mathbf{k}|^2 - 2\cos(\theta) + 1))^{D_f/2}} |\mathbf{k}|^2 \mathrm{d}|\mathbf{k}|. \tag{16}$$

Using Eqs. (14)–(16), μ_{sc} is expressed through C_0, l_c, D_f, and g as

$$\mu_{\mathrm{sc}} = \frac{k_0^2 \pi (1 + g^2 - g)^{3/2}}{1 - g^2} \int_0^{\infty} \frac{C_0}{[1 + (l_c k_0)^2 (|\mathbf{k}|^2 - 1)]^{D_f/2}} |\mathbf{k}|^2 \mathrm{d}|\mathbf{k}|. \tag{17}$$

This equation allows us to link medium parameters for the conventional MC and wave MC simulation and comparative analysis.

The reflection coefficient (reflectivity) of the layer with thickness δz is determined as follows:

$$\tilde{R}(\mathbf{r}_\perp, z) = \frac{\partial_z \tilde{n} \delta z}{2\tilde{n}}.$$

Note that this parameter characterizes the relationship between the amplitudes of the forward propagated $\tilde{A}$ and backscattered optical waves $\tilde{A}_{\mathrm{sc}}$: $\tilde{A}_{\mathrm{sc}} = \tilde{A}\sqrt{\tilde{R}}$.

3 Numerical Simulation

3.1 *Numerical Simulation Algorithm*

The splitting into physical processes approach was used for the numerical solution of Eqs. (4)–(6): at each step along the propagation direction, at first, the problem of free propagation is solved; then, the diffraction step alternates with the step of propagation through the phase screen describing the spatial distribution of the refractive index of the medium. Let us rewrite Eq. (4) in an operator form:

$$\frac{\partial}{\partial z} \tilde{U} = [\hat{\mathbf{D}} + \hat{\boldsymbol{T}}] \tilde{U},$$

where $\hat{\mathbf{D}} = \frac{i}{4} \nabla_\perp^2$ is the operator of the diffraction, $\hat{\boldsymbol{T}} = i\tilde{n}(\mathbf{r}_\perp, z)$ is the operator of passing the phase screen with propagation distance $h_z = \delta z$.

The optical wave transformation during the step δz along the propagation direction is represented as

$$\tilde{U}(z + \delta z) = \mathrm{e}^{\delta z \hat{\mathbf{D}}/2} (\mathrm{e}^{\delta z \hat{\boldsymbol{T}}} (\mathrm{e}^{\delta z \hat{\mathbf{D}}/2} (\mathrm{e}^{\delta z \hat{\boldsymbol{T}}/2} \tilde{U}(z)))). \tag{18}$$

The numerical scheme [Eq. (18)] is not completely conservative, and that can cause errors for strongly inhomogeneous media.[46] Therefore, a completely conservative numerical scheme had also been established.[47,48] In the framework of model media studied, both numerical schemes gave matching results.

The size of the skin inhomogeneities is of micron scale, and the diameter of the initial beam was selected of the 1 mm order. The depth of penetration of the optical wave into the biological tissue can be up to several hundred microns. To avoid the influence of boundary effects and take

Downloaded From: https://www.spiedigitallibrary.org/journals/Optical-Engineering on 09 Apr 2020
Terms of Use: https://www.spiedigitallibrary.org/terms-of-use

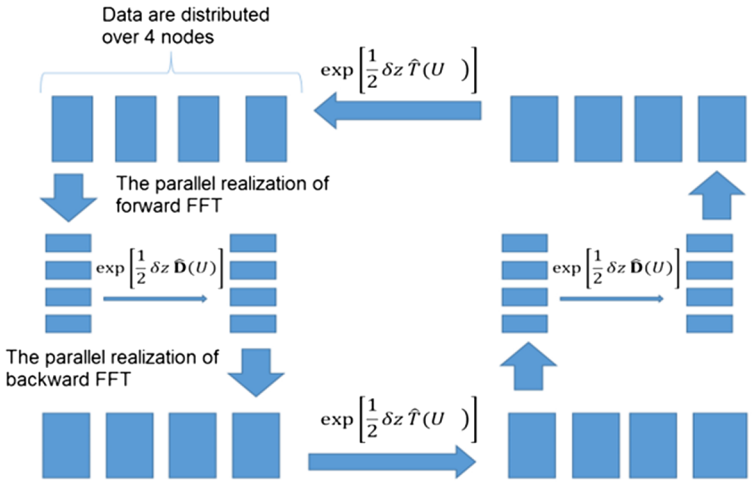

Fig. 1 Block diagram of calculation of an optical beam transformation for the step δz along the direction propagation, according to Eq. (18). The scheme corresponds to a case of four computational nodes.

into account the low-frequency spatial modes, which could appear during the wave propagation, the number of grid nodes was chosen as $4096 \times 4096 \times 1024$.

To speed up the calculations, we also used a slit-like beam transversal shape. The numerical scheme described in Ref. 49 was used to implement parallel computing. To do it, the spatial grid was decomposed according to one of the coordinates (along the coordinate of the narrow part of the slit beam) and, using the parallel version of the fast Fourier transform, the step of calculating the diffraction and the step of passing the phase screen through pointwise multiplication of arrays at each node were carried out. Figure 1 shows a block diagram of the computational algorithm.

The spatial distribution of the refractive index fluctuations was calculated, as shown in Ref. 37:

$$\delta\tilde{n} = \mathrm{Re}\left[\hat{F}^{-1}\left(\mathrm{Rand}\sqrt{C(\boldsymbol{k})/(8\pi N_x N_y N_z)}\right)\right] + \mathrm{Im}\left[\hat{F}^{-1}\left(\mathrm{Rand}\sqrt{C(\boldsymbol{k})/(8\pi N_x N_y N_z)}\right)\right]. \quad (19)$$

Here, $\hat{F}$ describes the fast Fourier transform operator; Rand is the random number generated for normal distribution with zero mean and unit variance; and N_x, N_y, N_z are the voxel numbers along the corresponding axes of the Cartesian coordinate system.

3.2 *Implementation Examples*

To compare the simulation results of recording the characteristics of biological tissue with a wave and particle OCT methods, we used a skin model with nevus,[4,5,12,50,51] which is used extensively in various modeling studies utilizing conventional MC. The relationship between the parameters of the microscopic model of a randomly inhomogeneous medium [Eq. (8)] and the scattering indicatrix used by the corpuscular MC was established according to Eq. (17) (see Fig. 2).

Figure 3 shows the results of the numerical simulation of biological tissue OCT visualization based on the skin with the nevus model presented in Fig. 2.

In the space area near coordinates (0.3, 0.5), a relatively bright structure is visible at the "basal layer–nevus–dermis" border, which is connected most likely with the optical wave focusing on the boundary between the granular and basal layers. The same structure is visible in the image obtained by the corpuscular MC method but with strong distortions compared to the wave method. The corpuscular MC simulation of a photon trajectory was conducted until the photon had been arrived at the plane of detector or absorbed. Dolganova et al.[12] used the total number of trajectories equal to 10^7. Evidently, MC simulations had been conducted on a very rough mesh. It seems that this is the main reason of the artifacts mentioned already.

Downloaded From: https://www.spiedigitallibrary.org/journals/Optical-Engineering on 09 Apr 2020
Terms of Use: https://www.spiedigitallibrary.org/terms-of-use

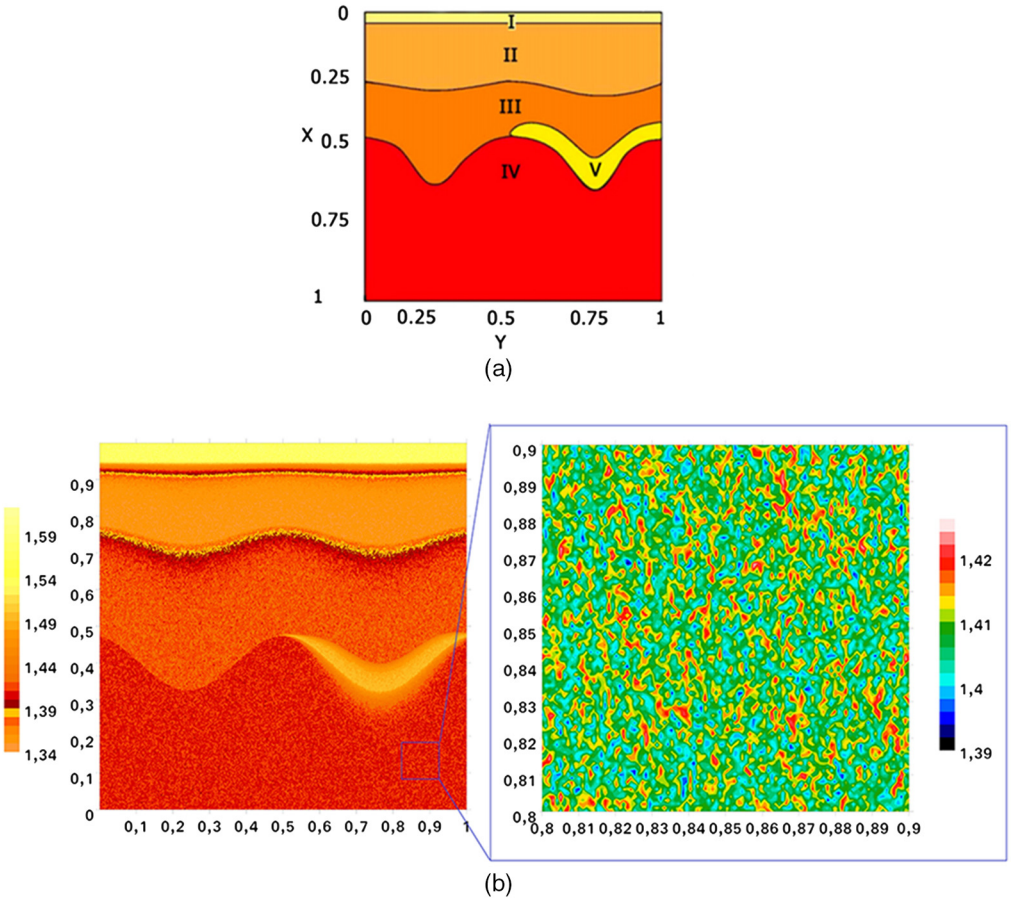

Fig. 2 A skin with a nevus model[12,49,50] (scales X and Y are normalized to 1 mm): (a) spatial distribution of media parameters: area I (upper stratum corneum): $n = 1.54$, $\mu_{sc} = 35$ mm^{-1}, $\mu_a = 0.02$ mm^{-1}, $g = 0.9$; $C_0 = 0.047$, $l_c = 1.5$ μm, $D_f = 3.9$; area II (epidermis, granular layer): $n = 1.34$, $\mu_{sc} = 5$ mm^{-1}, $\mu_a = 0.015$ mm^{-1}, $g = 0.95$; $C_0 = 0.021$, $l_c = 3.2$ μm, $D_f = 3.5$; area III (epidermis, basal layer): $n = 1.4$, $\mu_{sc} = 12$ mm^{-1}, $\mu_a = 0.02$ mm^{-1}, $g = 0.85$; $C_0 = 0.034$, $l_c = 1.05$ μm, $D_f = 3.7$; area IV (dermis): $n = 1.39$, $\mu_{sc} = 12$ mm^{-1}, $\mu_a = 0.1$ mm^{-1}, $g = 0.9$; $C_0 = 0.033$, $l_c = 1.6$ μm, $D_f = 3.8$; area V (nevus): $n = 1.38$, $\mu_{sc} = 7$ mm^{-1}, $\mu_a = 0.013$ mm^{-1}, $g = 0.8$; $C_0 = 0.02$, $l_c = 0.8$ μm, $D_f = 3.6$. (b) An example of the spatial distribution of the $\mathrm{Re}(\tilde{n}_c)$ implementation for the above parameter values (C_0, D_f, and l_c). On the sidebar: an example of the implementation of the spatial distribution of the refractive index calculated following Eq. (19).

Figure 4 shows the results of the numerical simulation of biological tissue OCT visualization using Bessel optical wave beams, which are diffracted minimally, using the model of skin with the nevus.

Figure 5(c) shows the diffraction spreading of the optical wave beam.[52] The quality of biological tissue OCT visualization using the Bessel optical wave beam with a transverse profile $J_0(20|\boldsymbol{r}_\perp|)$ is lower than for the case of the Bessel optical wave beam with a transverse profile $J_0(6|\boldsymbol{r}_\perp|)$.

Figure 5 shows an example of tissue OCT visualization for the case of the skin model shown in Fig. 2 in the absence of layer V (nevus).

The speckle noise was shown to increase under optical wave beam propagation in the tissue. It coincides, for example, with experimental results for a medium with suspensions of polystyrene microspheres.[6] The speckle image distortion is enhanced for optical wave beams with a more complicated transverse profile. The ability to evaluate such effects is a fundamental advantage of the proposed approach. It can be suitable for the optimization of an experimental implementation of the OCT.[53]

Downloaded From: https://www.spiedigitallibrary.org/journals/Optical-Engineering on 09 Apr 2020
Terms of Use: https://www.spiedigitallibrary.org/terms-of-use

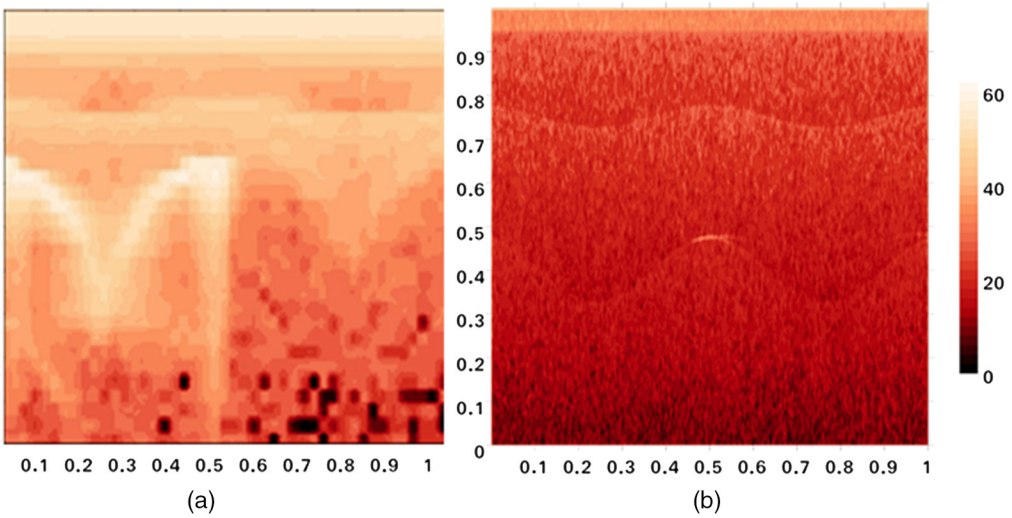

Fig. 3 The results of the numerical simulation of biological tissue OCT visualization based on the skin with the nevus model (Fig. 2; *X* and *Y* scales are normalized to 1 mm): (a) the implementation of the corpuscular MC method[12]; (b) the *a* of the MC wave method using a slit optical wave beam with a Gaussian profile with transverse dimensions of 1000 and 50 μm, the coherence length is 10 μm.

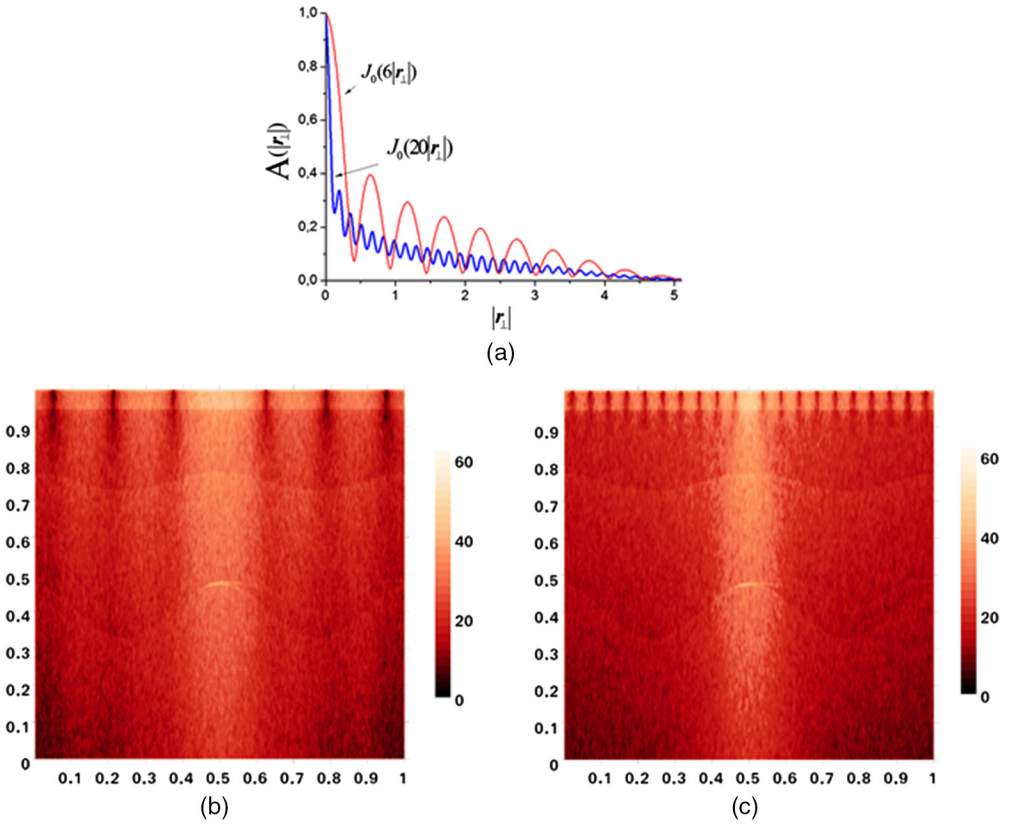

Fig. 4 The results of the numerical simulation of biological tissue OCT visualization based on the skin with the nevus model using Bessel optical wave beams with soft nullification on the edges of the mesh by super-Gaussian function (*X* and *Y* scales are normalized to 1 mm): (a) the transverse profiles of Bessel optical wave beam beams at the entrance to the medium; (b) the implementation of the MC wave method using the Bessel optical wave beam with a transverse profile $J_0(20|\mathbf{r}_\perp|)$, the coherence length is 10 μm; and (c) the implementation of the MC wave method using the Bessel optical wave beam with a transverse profile $J_0(6|\mathbf{r}_\perp|)$, the coherence length is 10 μm.

Downloaded From: https://www.spiedigitallibrary.org/journals/Optical-Engineering on 09 Apr 2020
Terms of Use: https://www.spiedigitallibrary.org/terms-of-use

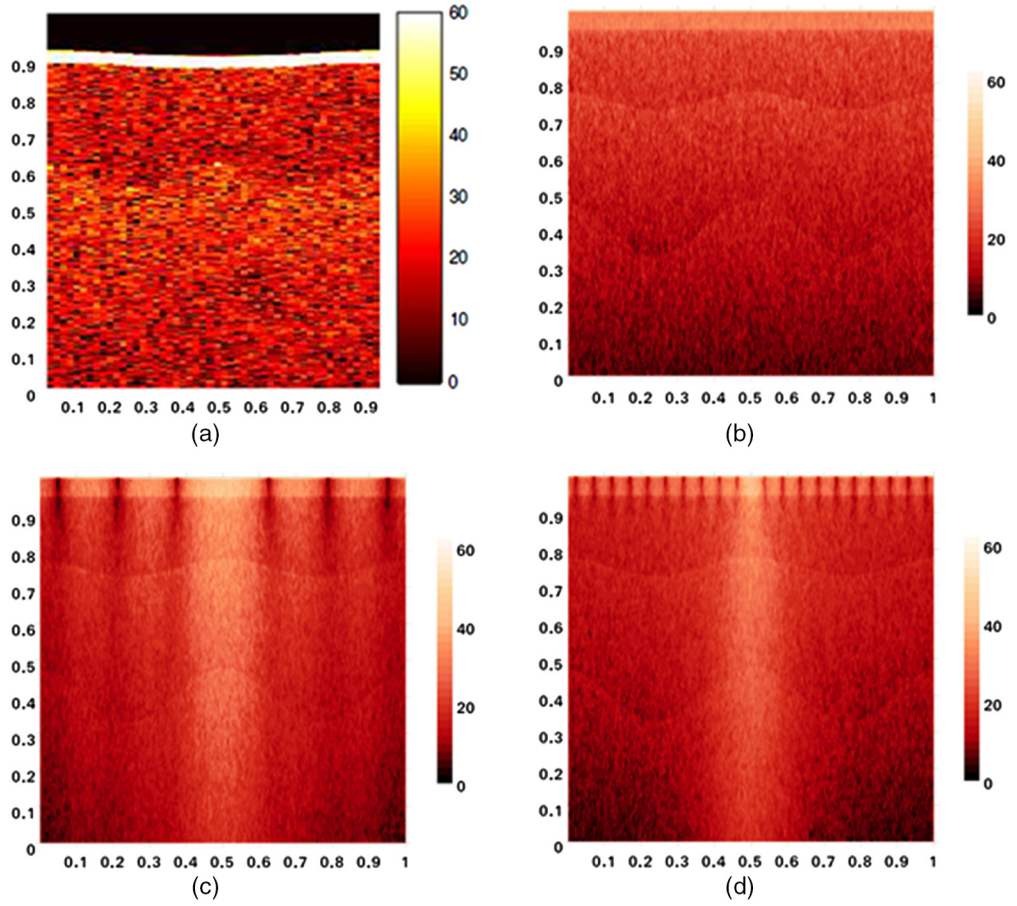

Fig. 5 The results of the numerical simulation of biological tissue OCT visualization based on the skin model without the nevus (see Fig. 2; X and Y scales are normalized to 1 mm): (a) the implementation of the corpuscular MC method, the coherence length is 10 μm[50]; (b) the implementation of the MC wave method using a slit optical wave beam with a Gaussian profile with transverse dimensions of 1000 and 50 μm, the coherence length is 10 μm; (c) the implementation of the MC wave method using a Bessel optical wave beam with a transverse profile $J_0(20|\mathbf{r}_\perp|)$, the coherence length is 10 μm; and (d) the implementation of the MC wave method using a Bessel optical wave beam with a transverse profile $J_0(6|\mathbf{r}_\perp|)$, the coherence length is 10 μm.

4 Summary and Conclusion

We introduce a computational modeling approach specially developed for mimicking the time-domain OCT images of biotissues. The developed modeling technique is based on the implementation of the Leontovich–Fock equation into the wave MC method. The selection of optical parameters of modeling medium, used for simulation of optical radiation propagation in biotissues, is based on the results obtained experimentally by OCT. The developed computational modeling approach allows one to take into account diffraction effects on bulk, absorbing objects and the influence of the amplitude–phase profile of the wave beam on the quality of OCT imaging. The limitations of the approach are associated, first of all, with the conditions of applicability of the parabolic equation used. The accuracy of the latter is determined by the value of the numerical aperture, which should be much less than unity within the framework of the quasioptics approximation. Secondly, the presented results were obtained without multiple scattering. The speed of the numerical implementation essentially depends on the available computing resources and the optimization of the numerical scheme. Simulation of the time-domain OCT images presented in the current version of the MC model on a computer with 24 processors takes 3 to 4 h. The developed computational model can be used for imitation of the light waves propagation both in time-domain and spectral-domain OCT approaches.

Downloaded From: https://www.spiedigitallibrary.org/journals/Optical-Engineering on 09 Apr 2020
Terms of Use: https://www.spiedigitallibrary.org/terms-of-use

Acknowledgments

This work was done using resources of the Collective Use Center, Siberian Super Computer Center of the Siberian Branch of the Russian Academy of Sciences. This work was partly supported by the Russian Foundation for Basic Research (Grant No. 17-00-00186), RFBR, and Administration of Tomsk Region (Grant Nos. 18-42-703012 and 18-41-703004). This work was carried out in the framework of the Fundamental Scientific Research Program of the State Academies of Sciences for 2013-2020, direction III.23.2.10. A.D.B., D.A.V., E.S.S., I.M., and Yu.V.K. have nothing to disclose.

References

1. A. L. Matveyev et al., "Semi-analytical full-wave model for simulations of scans in optical coherence tomography with accounting for beam focusing and the motion of scatterers," *Laser Phys. Lett.* **16**(8), 085601 (2019).
2. J. Kalkman, "Fourier-domain optical coherence tomography signal analysis and numerical modeling," *Int. J. Opt.* **2017**, 1–16 (2017).
3. M. Jensen et al., "All-depth dispersion cancellation in spectral-domain optical coherence tomography using numerical intensity correlations," *Sci. Rep.* **8**, 9170 (2018).
4. D. Y. Churmakov, V. L. Kuzmin, and I. Meglinski, "Application of the vector Monte Carlo method in polarization optical coherence tomography," *Quantum Electron.* **36**(11), 1009–1015 (2006).
5. I. Meglinski et al., "Simulation of polarization-sensitive optical coherence tomography images by a Monte Carlo method," *Opt. Lett.* **33**(14), 1581–1583 (2008).
6. M. Y. Kirillin et al., "Speckle statistics in OCT images: Monte Carlo simulations and experimental studies," *Opt. Lett.* **39**(12), 3472–3475 (2014).
7. Y. Pan et al., "Low-coherence optical tomography in turbid tissue: theoretical analysis," *Appl. Opt.* **34**(28), 6564–6574 (1995).
8. D. J. Smithies et al., "Signal attenuation and localization in optical coherence tomography studied by Monte Carlo simulation," *Phys. Med. Biol.* **43**(10), 3025–3044 (1998).
9. G. Yao and L. V. Wang, "Monte Carlo simulation of an optical coherence tomography signal in homogeneous turbid media," *Phys. Med. Biol.* **44**(9), 2307–2320 (1999).
10. A. Tycho et al., "Derivation of a Monte Carlo method for modeling heterodyne detection in optical coherence tomography systems," *Appl. Opt.* **41**(31), 6676–6691 (2002).
11. Q. Lu et al., "Monte Carlo modeling of optical coherence tomography imaging through turbid media," *Appl. Opt.* **43**(8), 1628–1637 (2004).
12. I. Dolganova et al., "Monte Carlo simulation of optical coherence tomography signal of the skin nevus," *J. Phys. Conf. Ser.* **673**, 012014 (2016).
13. B. Hokr et al., "Modeling focusing Gaussian beams in a turbid medium with Monte Carlo simulations," *Opt. Express* **23**, 8699–8705 (2015).
14. C. K. Hayakawa, E. O. Potma, and V. Venugopalan, "Electric field Monte Carlo simulations of focal field distributions produced by tightly focused laser beams in tissues," *Biomed. Opt. Express* **2**(2), 278–290 (2011).
15. Y. Wang and L. Bai, "Accurate Monte Carlo simulation of frequency-domain optical coherence tomography," *Int. J. Numer. Methods Biomed. Eng.* **35**(4), e3177 (2019).
16. L. Thrane, H. T. Yura, and P. E. Andersen, "Analysis of optical coherence tomography systems based on the extended Huygens-Fresnel principle," *J. Opt. Soc. Am. A* **17**, 484–490 (2000).
17. J. M. Schmitt and A. Knüttel, "Model of optical coherence tomography of heterogeneous tissue," *J. Opt. Soc. Am. A* **14**(6), 1231–1242 (1997).
18. M. R. N. Avanaki et al., "Quantitative evaluation of scattering in optical coherence tomography skin images using the extended Huygens-Fresnel theorem," *Appl. Opt.* **52**(8), 1574–1580 (2013).
19. D. P. Popescu and M. G. Sowa, "*In vitro* assessment of optical properties of blood by applying the extended Huygens-Fresnel principle to time-domain optical coherence tomography signal at 1300 nm," *Int. J. Biomed. Imaging* **2008**, 1–6 (2008).

Downloaded From: https://www.spiedigitallibrary.org/journals/Optical-Engineering on 09 Apr 2020
Terms of Use: https://www.spiedigitallibrary.org/terms-of-use

20. L. Chin et al., "Analysis of image formation in optical coherence elastography using a multiphysics approach," *Biomed. Opt. Express* **5**(9), 2913–2930 (2014).
21. L. Thrane et al., "Extraction of tissue optical properties from optical coherence tomography images for diagnostic purposes," *Proc. SPIE* **5771**, 139–150 (2005).
22. A. Tycho, T. M. Joergensen, and L. Thrane, "Focusing problem in OCT: comparison of Monte-Carlo simulations, the extended Huygens-Fresnel principle, and experiments," *Proc. SPIE* **3915**, 25–35 (2000).
23. B. Simon and C. A. DiMarzio, "Simulation of a theta line-scanning confocal microscope," *J. Biomed. Opt.* **12**, 064020 (2007).
24. S. Lee and J. P. Rolland, "Bessel beam spectral-domain high-resolution optical coherence tomography with micro-optic axicon providing extended focusing range," *Opt. Lett.* **33**(15), 1696–1698 (2008).
25. L. Yi et al., "Multifocal spectral-domain optical coherence tomography based on Bessel beam for extended imaging depth," *J. Biomed. Opt.* **22**(10), 106016 (2017).
26. L. Yi, L. Sun, and X. Ming, "Simulation of penetration depth of Bessel beams for multifocal optical coherence tomography," *Appl. Opt.* **57**(17), 4809–4814 (2018).
27. P. R. T. Munro, "Three-dimensional full wave model of image formation in optical coherence tomography," *Opt. Express* **24**(23), 27016–27031 (2016).
28. D. C. Reed and C. A. DiMarzio, "Computational model of OCT in lung tissue," *Proc. SPIE* **7570**, 75700I (2010).
29. A. S. F. C. Silva and A. L. Correia, "From optical coherence tomography to Maxwell's equations," in *IEEE 3rd Portuguese Meeting Bioeng.*, pp. 1–4 (2013).
30. P. Ossowski et al., "Realistic simulation and experiment reveals the importance of scatterer microstructure in optical coherence tomography image formation," *Biomed. Opt. Express* **9**(7), 3122–3136 (2018).
31. F. Devaux and E. Lantz, "3D-PSTD simulation and polarization analysis of a light pulse transmitted through a scattering medium," *Opt. Express* **21**(21), 24969–24984 (2013).
32. Q. H. Liu, "The PSTD algorithm: a time-domain method requiring only two cells per wavelength," *Microwave Opt. Technol. Lett.* **15**(3), 158–165 (1997).
33. G. Gbur, "Partially coherent beam propagation in atmospheric turbulence," *J. Opt. Soc. Am. A* **31**(9), 2038–2045 (2014).
34. M. A. Leontovich and V. A. Fock, "Solution of the problem of propagation of electromagnetic waves along the earth's surface by method of parabolic equations," *J. Phys. USSR* **10**, 13–23 (1946).
35. V. P. Kandidov et al., "Application of corpuscular and wave Monte-Carlo methods in optics of dispersive media," *Quantum Electron.* **36**(11), 1003–1008 (2006).
36. S. A. Akhmanov, Y. E. Dyakov, and A. S. Chirkin, *Introduction in Statistical Radiophysics and Optics*, Nauka, Moscow (1981).
37. A. K. Glaser, Y. Chen, and J. T. C. Liu, "Fractal propagation method enables realistic optical microscopy simulations in biological tissues," *Optica* **3**(8), 861–869 (2016).
38. J. D. Rogers et al., "Modeling light scattering in tissue as continuous random media using a versatile refractive index correlation function," *IEEE J. Sel. Top. Quantum Electron.* **20**(2), 173–186 (2014).
39. M. Xu and R. Alfano, "Fractal mechanisms of light scattering in biological tissue and cells," *Opt. Lett.* **30**(22), 3051–3053 (2005).
40. M. Xu, T. T. Wu, and J. Y. Qu, "Unified Mie and fractal scattering by cells and experimental study on application in optical characterization of cellular and subcellular structures," *J. Biomed. Opt.* **13**(2), 024015 (2008).
41. T. T. Wu, J. Y. Qu, and M. Xu, "Unified Mie and fractal scattering by biological cells and subcellular structures," *Opt. Lett.* **32**(16), 2324–2326 (2007).
42. C. J. Sheppard, "Fractal model of light scattering in biological tissue and cells," *Opt. Lett.* **32**(2), 142–144 (2007).
43. N. Das et al., "Tissue multifractality and Born approximation in analysis of light scattering: a novel approach for precancers detection," *Sci. Rep.* **4**, 6129 (2015).
44. L. G. Henyey and J. L. Greenstein, "Diffuse radiation in the galaxy," *Astrophys. J.* **93**, 70–83 (1941).

Downloaded From: https://www.spiedigitallibrary.org/journals/Optical-Engineering on 09 Apr 2020
Terms of Use: https://www.spiedigitallibrary.org/terms-of-use

45. T. Binzoni et al., "The use of the Henyey-Greenstein phase function in Monte Carlo simulations in biomedical optics," *Phys. Med. Biol.* **51**, N313–N322 (2006).
46. A. D. Bulygin and A. A. Zemlyanov, "Variational statement of the Schrödinger equation with a nonstationary nonlinearity and its integrals of motion," *Differ. Equations* **54**(10), 1394–1398 (2018).
47. A. D. Bulygin and D. A. Vrazhnov, "A fully conservative parallel numerical algorithm with adaptive spatial grid for solving nonlinear diffusion equations in image processing," *Supercomput. Front. Innovations* **6**(1), 9–13 (2019).
48. A. D. Bulygin, "Algorithm of the parallel sweep method for numerical solution of the gross-Pitaevskii equation with highest nonlinearities," *Supercomput. Front. Innovations* **5**(4), 115–118 (2018).
49. A. A. Voronin and A. Zheltikov, "Nonlinear dynamics of high-power ultrashort laser pulses: exaflop computations on a laboratory computer station and subcycle light bullets," *Phys. Usp.* **59**(9), 869–877 (2016).
50. M. Y. Kirillin, A. V. Priezzhev, and R. Myllylä, "Role of multiple scattering in formation of OCT skin images," *Quantum Electron.* **38**(6), 570–575 (2008).
51. M. Kirillin et al., "Simulation of optical coherence tomography images by Monte Carlo modeling based on polarization vector approach," *Opt. Express* **18**(21), 21714–21724 (2010).
52. P. Porfirev and R. V. Skidanov, "Generation of an array of optical bottle beams using a superposition of Bessel beams," *Appl. Opt.* **52**(25), 6230–6238 (2013).
53. A. F. Fercher et al., "Optical coherence tomography-principles and applications," *Rep. Prog. Phys.* **66**(2), 239–303 (2003).

Igor Meglinski is a professor at the University of Oulu (Finland) and Aston University (UK). His research interests lie at the interface between physics, medicine, and biological sciences, focusing on the development of new noninvasive imaging/diagnostic techniques and their application in medicine and biology, material sciences, pharmacy, food, environmental monitoring, and health care industries. He is the author and coauthor of over 350 research papers in peer-reviewed scientific journals, proceedings of international conferences, and book chapters, and over 650 presentations at the major international conferences and symposia in the field, including over 290 invited lectures and plenary talks. He is a chartered physicist (CPhys), a chartered engineer (CEng), a fellow of Institute of Physics (FInstP), and a fellow of SPIE.

Yury V. Kistenev is a professor at Tomsk State University (TSU). He received his PhD in optics in 1987 and his doctor degree in physics and mathematics in 1997. He is the author of more than 140 journal papers and has written two book chapters. His current research interests include laser molecular imaging, laser spectroscopy, and machine learning. He is a member of SPIE.

Biographies of the other authors are not available.

Downloaded From: https://www.spiedigitallibrary.org/journals/Optical-Engineering on 09 Apr 2020
Terms of Use: https://www.spiedigitallibrary.org/terms-of-use